

An Extension of the GISSMO Damage Model Based on Lode Angle Dependence

¹⁾ Merdan Basaran, ¹⁾ Sven David Wölkerling, ¹⁾ Markus Feucht, ¹⁾ Frieder Neukamm, ²⁾ Dieter Weichert

¹⁾ DAIMLER AG, Sindelfingen, Germany

²⁾ RWTH, Aachen, Germany

Abstract:

This paper presents the extension and validation of the damage model GISSMO (Generalized Incremental Stress State dependant damage MOdel). The damage model is extended for 3D usage by utilization of Lode angle parameter. The fracture strain is defined in the stress triaxiality and Lode angle parameter space as a surface. The fracture strain definition is introduced as a table definition.

The stress triaxiality and Lode angle parameter space is covered with proper specimens and load conditions. The validation is done for dual phase steel DP600. Round specimens, flat-grooved plane strain specimens with different notches and Nakazima biaxial specimens are used to get information for the Lode angle parameter values 1, 0 and -1, respectively. Additionally butterfly and flat tension specimens are used in order to cover intermediate stress states.

The focus of the paper is the introduction of a calibration approach using numerical simulation and comparison with experimental results of specimens. The simulations were performed using LS-DYNA and an extended version of the GISSMO model.

Keywords:

Lode dependence, Pressure effect, Fracture Locus, Calibration Method

1 Introduction

In recent years, great effort has been spent in order to improve crashworthiness of car body structures. The importance of simulations of these structures has increased significantly since it is an efficient way to reduce costly experiments. The simulation of structures under crash loads requires complex material and damage models since the material is loaded beyond ultimate stress to fracture.

From micromechanical point of view, ductile failure of material is defined as material separation which is the result of void nucleation and evolution of existing micro voids and cracks, followed by progressive void coalescence. Macroscopically damage is defined as the loss of ductility of material. Various numerical models are suggested to model fracture (crack) initiation and propagation. These models can be discussed mainly in three groups: Uncoupled continuum models (I), micromechanical models (II) and continuum damage models (CDM) (III). In the first group, damage is defined by an external variable which is uncoupled from plasticity internal variables. In this case, the damage variable does not affect plastic properties of the material and the material fails when damage variable reaches its critical value as in Johnson-Cook [1] and Wilkins [2] models. In the second group material is handled as inhomogeneous cells with consideration of voids and micro cracks. Macroscopic material response is determined by the global response of void containing cell. For this group Rousselier [3] and Gurson [4] model can be given as example. In the third group, void growth and their interactions are described in a phenomenological way. The damage variable is coupled with plasticity internal variables in order to model stiffness degradation (see for example Lemaitre's [5] and Xue's [6] models).

Contrary to pressure or as commonly used stress triaxiality dependence, Lode angle dependence (or the third deviatoric stress invariant) on ductile metal failure did not get enough attention. Recently Wierzbicki et al. [7] covered a wide range of Lode angle parameter and stress triaxiality range with proper specimens to show the influence of the Lode angle on the fracture strain. Numerical damage models incorporating Lode dependence are proposed by many researchers. Incorporating Lode angle dependence, Barsoum et al. [8] extended Rice's micromechanical model; Xue[9], Nahson and Hutchinson [10] modified the existing Gurson-Tveergard-Needleman model. Bai and Wierzbicki [11] proposed a continuum damage model with Lode angle dependence.

In this paper the damage model GISSMO (Generalized Incremental Stress State dependant damage MOdel) proposed by Neukamm et al. [12-13] is extended to incorporate the Lode angle dependence for 3D-case. Dual phase steel (DP600) is investigated under different stress states (stress triaxiality and Lode angle parameter combinations). The stress triaxiality - Lode angle parameter space is covered with several different type of specimens; flat, round-axisymmetric, flat-grooved, butterfly and Nakazima specimens. A calibration approach is proposed for the fracture locus in stress triaxiality, Lode angle parameter and fracture strain. It is shown that Lode angle has significant influence on the fracture strain of DP600 steel.

2 Stress State Variables

The stress state of a material point can be represented in principal stress space $[\sigma_1, \sigma_2, \sigma_3]$ called Haigh-Westergaard stress space (Fig. 1). The stress state of a material point can be also described in cylindrical coordinate system $[\sigma_{eq}, \theta, \sigma_m]$. Equivalent stress (von Mises stress) σ_{eq} and mean stress σ_m are defined, respectively by

$$\sigma_{eq} = \frac{1}{\sqrt{2}} \sqrt{(\sigma_1 - \sigma_2)^2 + (\sigma_1 - \sigma_3)^2 + (\sigma_2 - \sigma_3)^2}, \quad (1.)$$

$$\sigma_m = \frac{1}{3} (\sigma_1 + \sigma_2 + \sigma_3). \quad (2.)$$

Angle θ shows the Lode dependence (Fig.1). The three cylindrical coordinates can be also expressed with three stress invariants I_1, J_2, J_3 , which are first stress invariant, second and third deviatoric stress invariants, respectively

$$\sigma_{eq} = \sqrt{3J_2}, \quad (3.)$$

$$\sigma_m = \frac{1}{3}I_1, \quad (4.)$$

$$\theta = \frac{1}{3} \arccos\left(\frac{3\sqrt{3}}{2} \frac{J_3}{J_2^{3/2}}\right). \quad (5.)$$

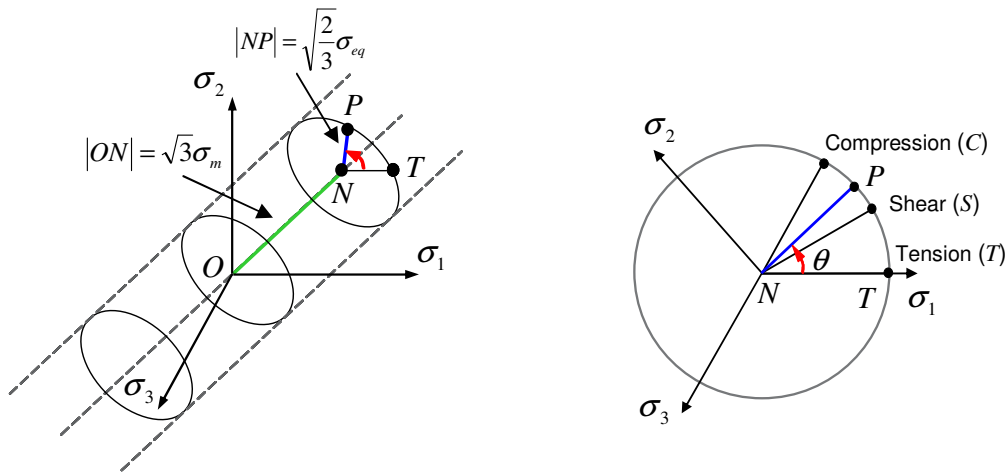


Figure 1: Stress state representation in Cartesian and cylindrical coordinate systems

The dimensionless parameter, stress triaxiality is used commonly as a measure defining the ductility of a material and it has been correlated directly to the fracture strain by many researchers [1,14-16]. Stress triaxiality is defined as the ratio of mean stress and equivalent stress

$$\eta = \frac{\sigma_m}{\sigma_{eq}} = \frac{1/3 I_1}{\sqrt{3J_2}}. \quad (6.)$$

The Lode angle θ is also normalized and dimensionless Lode angle parameter ξ is defined through

$$\xi = \cos(3\theta) = \frac{27}{2} \frac{J_3}{\sigma_{eq}^3} = \frac{3\sqrt{3}}{2} \frac{J_3}{J_2^{3/2}}. \quad (7.)$$

A detailed derivation is presented in [17]. It should be noted that stress triaxiality is a relation of stress invariants I_1 and J_2 and Lode angle parameter is formulated with stress invariants J_2 and J_3 . Under proportional loading, the stress triaxiality and the Lode angle parameter remain constant on the loading path.

Xue and Wierzbicki [18] showed that for plane stress state ($\sigma_3 = 0$) there is a unique relation between stress triaxiality and Lode angle parameter as

$$\xi = -\frac{27}{2} \eta \left(\eta^2 - \frac{1}{3} \right). \quad (8.)$$

3 Damage Evolution Rule

Damage is a complex phenomenon and it is claimed that it should be defined as a tensor quantity [19-21]. In this case experimental determination of damage parameters is a very complicated and difficult task. In many industrial applications damage indicator is assumed as a scalar value and also good results are obtained. In the GISSMO model, damage is defined by scalar value in a phenomenological way through a power equation

$$D = \left(\frac{\varepsilon_p}{\varepsilon_f} \right)^n, \quad (9.)$$

where ε_p is the equivalent plastic strain, ε_f is the equivalent plastic strain at fracture (fracture strain) depending on the stress state parameters stress triaxiality and Lode angle parameter and n is the damage exponent. It should be noted Eq. (9) is only valid for proportional loading. The definition can be expressed in incremental form through

$$dD = \frac{n}{\varepsilon_f(\eta, \xi)} D^{\frac{n-1}{n}} d\varepsilon_p = f(D, \varepsilon_f) d\varepsilon_p, \quad (10.)$$

where f is a function of current damage, stress state dependent fracture strain and damage exponent. It should be also noted that for the damage increment calculation, current damage of the material point is used. For complex loading histories the damage increment is integrated as

$$D = \int f(D, \varepsilon_f) d\varepsilon_p \leq 1. \quad (11.)$$

In the GISSMO damage model the lower limit of the integral can be defined explicitly. For the current research, under proportional loading the initial and end conditions are assumed as $D = 0$ at $\varepsilon_p = 0$ and $D = 1$ at $\varepsilon_p = \varepsilon_f$. With these boundary conditions Eq. (9) defines infinitely many solution functions depending on damage exponent.

4 Experimental Program

A wide range of stress state is covered with different types of specimens. The specimens are machined from the dual phase steel DP600 sheet with 2mm thickness. All the specimens are machined from rolling direction. The investigation for DP600 steel with 1.5mm sheet thickness shows that the in-plane anisotropy of the material is not significant [22]. In this paper the material is assumed to be isotropic. The loading environment is quasi-static loading.

The experimental program consists of flat, round, flat-grooved, Nakazima and Butterfly specimens. The flat, round and flat-grooved specimens are machined and tested at IWM-Freiburg. The Nakazima specimens and butterfly specimens are tested at IKH-Aachen and at IAM-Aachen (RWTH), respectively. The scope of the experimental program is shown in Fig.2.

Flat specimens consist of a smooth and two notched specimens with radii of R4mm and R2mm. The width (w) and thickness (t) of the minimum section is 5 and 2 mm, respectively. The gauge length for smooth specimen is 10mm and for the notched specimens 30mm.

The round notched specimens are used in order to investigate fracture strain for different stress triaxiality values under constant Lode angle parameter $\xi = 1$ (Fig. 3). Four geometries with notches 0.5mm, 1mm, 2mm and 4mm were tested. The diameter of maximum and minimum cross section at the notch is 1.8mm and 1mm, respectively. For all round specimens, gauge length 10mm is used.

The third group is double side flat-grooved plane strain specimens with radii of grooves 0.5mm, 1mm, 2mm and 4mm. This group of specimens is used in order to investigate fracture strain under plane strain conditions which corresponds to Lode angle parameter $\xi = 0$, where strain component in width direction is negligibly small compared to other principal directions. The ratio of width/thickness at groove is an important measure for plane strain specimens since for lower ratios the stress state will change towards axisymmetric stress state. Hancock [23] and Bai [11] used width/thickness ratio 8 and

31.25 at groove, respectively. The effect of depth of the groove is also investigated with FE-Simulations. It has been observed that depth of the groove has also an important influence on the stress state. With consideration of machining abilities and machined sheet, at the groove 10mm width and 0.8mm thickness ($w/t=12.5$) is assigned to flat-grooved specimens. The thickness of the maximum cross section is 2mm which corresponds to maximum thickness / minimum thickness of 2.5. For each flat-grooved specimen gauge length 20mm is used.

Nakazima specimens are used to investigate mainly the biaxial stress state. Two different geometries with 70mm and 90mm were tested (Fig. 3). The specimen with 90mm width is considered to have biaxial stress state which corresponds to stress triaxiality $2/3$ and Lode angle parameter -1 .

The last group is butterfly specimens and they are used to cover a wide range on the stress triaxiality - Lode angle parameter space with different loading directions. Mohr et. al [24] used butterfly shaped specimens in order to investigate fracture strain in the range $\eta = 0-0.6$ of stress triaxiality. Bai and Wierzbicki [11] calibrated with butterfly specimens the fracture locus in stress triaxiality and Lode angle parameter space. The butterfly specimen has a unique shape and there is strain concentration at the centre of the specimen for all load cases. The minimum thickness at the centre is 1 mm. With one specimen geometry it is possible to cover a wide range in the stress triaxiality - Lode angle parameter space (Fig. 3). The specimens were tested under 5 different loading directions, -10° , 0° , 10° , 20° and 60° (Fig. 2).

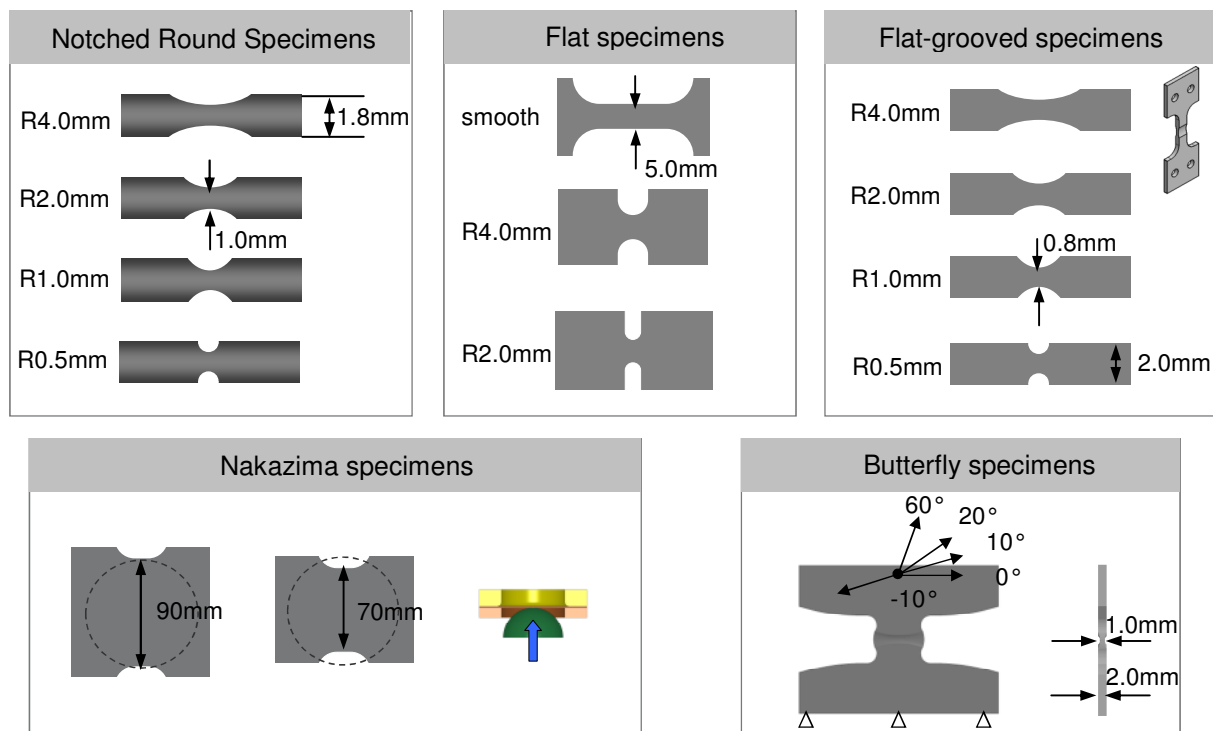


Figure 2: Experimental program: Notched round, flat, flat-grooved, Nakazima and butterfly specimens

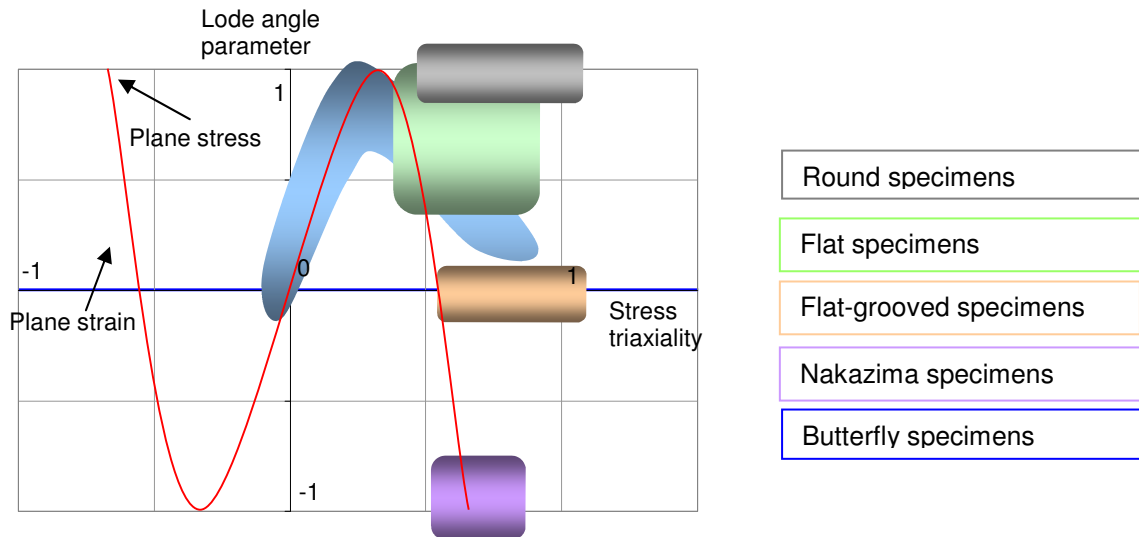


Figure 3: Stress states covered by different specimen types

5 Calibration of Fracture Locus

Calibration of fracture locus is done in two steps. In this paper an uncoupled formulation is used. In the first step the stress-strain curve is extracted from the flat smooth specimen. In the second step the histories of the stress state parameters for crack initiation locations are determined. Weighting functions are used in order to define a specific point for each specimen in the stress triaxiality, Lode angle parameter and fracture strain space.

5.1 FE - discretization

In order to investigate physical measures, stress triaxiality, Lode angle parameter and equivalent strain to fracture fine mesh has been used. To have reasonable calculation times a convergence analysis for flat specimens (smooth and notched R2mm, R4mm) is carried out and it is observed that numerical results (global force-displacement response, equivalent plastic strain, stress triaxiality and Lode angle parameter histories) converge at element length 0.1mm. Thus for the critical locations as the maximum element length 0.1mm is used. Only exception is Nakazima specimen with 0.2mm for the critical locations because of the specimen dimensions. In consideration of FE-calculation times the symmetry conditions are considered; the flat, round and flat-grooved specimens are modelled as 1/8, Nakazima specimens as 1/4 and butterfly specimens as 1/2 of real geometries. On the critical locations with strain concentration and high gradients almost 1/1 aspect ratio of the elements has been kept. In all simulations fully integrated 8-Node brick elements (Type 2) are used. The finite element discretization at critical location for butterfly specimen is shown in Fig. 4.



Figure 4: Finite element discretization of butterfly specimen at the critical location (centre)

5.2 Stress - strain curve

CDM and micromechanical models use the stress-strain curve for the matrix material, which represents the undamaged part of a representative volume element (RVE). However the experimentally measured curve is the combination of both material hardening and damaging effects. Experimentally the separation of damage and plastic flow is not possible. In this paper, damage is considered as a variable separated from the plastic flow. The stress-strain curve obtained from experiment has been used in the plasticity formulation directly.

In order to determine the stress-strain curve, flat smooth specimen is used. The output of the experiment is engineering stress and engineering strain which are determined through

$$\sigma_E = \frac{F}{A_0}, \quad (12.)$$

$$\varepsilon_E = \frac{L - L_0}{L_0} = \frac{\Delta L}{L_0}, \quad (13.)$$

where F is the measured axial force, A_0 is the initial cross section area of the specimen. L and L_0 are the measured length and initial length of the gauge. The quantities σ_E and ε_E can be transformed to true stress σ_t and strain ε_t by

$$\sigma_t = \sigma_E (1 + \varepsilon_E), \quad (14.)$$

$$\varepsilon_t = \ln(\varepsilon_E + 1). \quad (15.)$$

It should be noted that the relations in Eq. (15, 16.) can be used only up to the onset of necking since stress state for all material points on the critical cross section remains approximately uniaxial. In this case stress tensor has only one component (σ_t) and equivalent stress is equal to this component. With the assumption of incompressibility the equivalent plastic strain is equal to the plastic strain component (ε_t) in axial direction in plastic strain tensor. However beyond necking the above mentioned relations cannot be used directly because deformation is not uniform at the necking location. After necking the stress-strain curve can be extrapolated with phenomenological relations ([25-26]). For the extrapolation of the stress-strain curve beyond the necking the power law of Ludwik [27]

$$\sigma_w = A + B\varepsilon_p^n, \quad (16.)$$

has been used. The calibrated true stress-strain curve ($\sigma_t - \varepsilon_t$) and the engineering stress-strain curve ($\sigma_E - \varepsilon_E$) curve are shown in the Fig. 5.

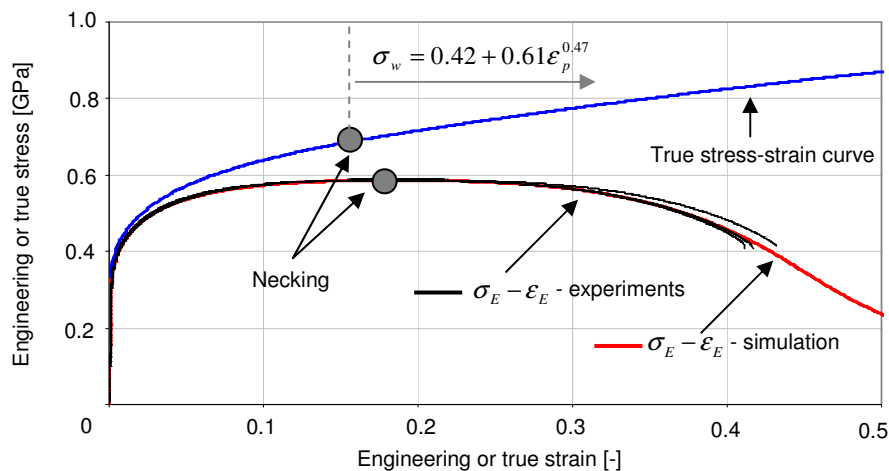


Figure 5: Engineering and true stress-strain curves

5.3 Determination of Fracture Strain in Triaxiality and Lode angle space

The fracture strain is defined as a surface in the third dimension over the plane of stress triaxiality and Lode angle parameter. Each specimen represents a unique point in 3D space and fracture surface is constructed on these points. In order to determine the mentioned quantities a mixed method, which combines the numerical simulation and experiments is used. From experiments global force-displacement curves are obtained. Parallel numerical simulations are carried out in order to obtain global force-displacement responses and the components of stress and strain tensors on the specimen. The material is assumed to reach its fracture strain at the location of crack initiation. In order to determine fracture strain, global displacement to crack initiation obtained from experiments are related to equivalent plastic strain at crack initiation location in numerical simulations. The evolution of stress triaxiality and Lode angle parameter at the crack initiation location are also extracted from numerical simulations.

The fracture initiation location can be observed optically. However sometimes it can be a very challenging task since cracks can be initiated inside the specimen or propagate very fast during loading. In this case the two questions have to be answered; where and at which global displacement the fracture initiates. The crack initiation location for specimens can be investigated experimentally by interrupting the tests at different displacement levels and slicing the specimen followed by examination with a microscope. This approach has been used by some researchers for the investigation of round specimens and it has been found that crack initiate at the centre of the specimen where stress triaxiality and equivalent plastic strain are the largest [23]. The experimental force-displacement responses can also give information about displacement to fracture. Usually there is a significant drop as the crack initiates [16]. In this research it is assumed that fracture process is very fast and the global displacement difference between crack initiation and significant amount of material failure is small.

The observation of crack initiation location is not an easy task for flat, round and flat-grooved specimens. For these three types of specimens, during the loading process, equivalent plastic strain and stress triaxiality values are highest at the centre of notches and grooves. Thus the crack is assumed to initiate at these material points. The equivalent plastic strain and stress triaxiality histories for three different points of the flat-grooved specimen with groove R1mm is shown in Fig. 6. The normalized force (F/A_0), stress triaxiality and equivalent plastic strain are related to global normalized displacement ($\Delta L/L_0$). It is shown that the equivalent plastic strain and stress triaxiality are the highest at the center (Point A) of the specimen.

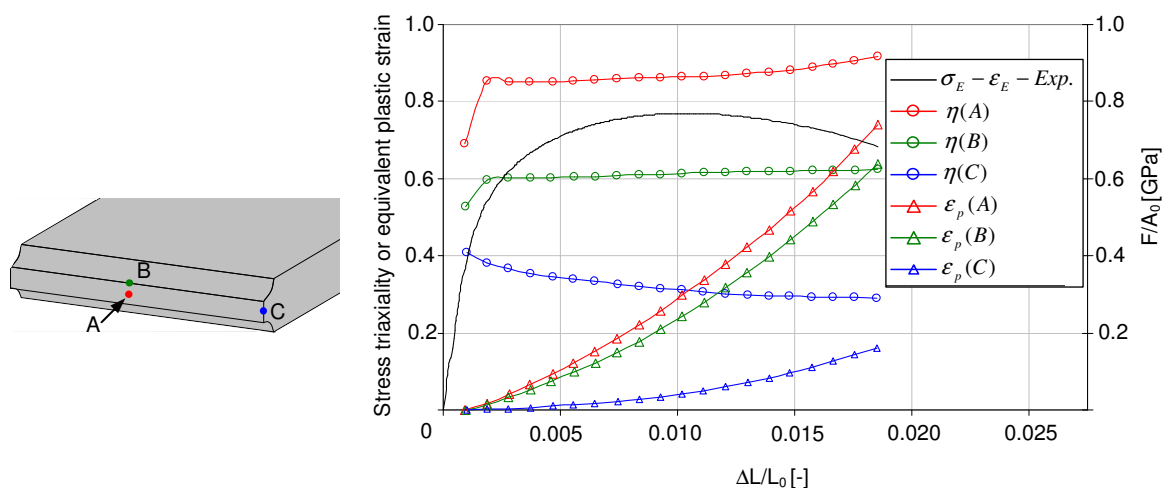


Figure 6: History of stress triaxiality and equivalent plastic strain at point A, B, C at minimum cross section of flat grooved specimen R1mm

There is a strain concentration at centre of butterfly specimens for all loading angles (Fig. 7), but usually it is not possible to observe the exact location of the crack initiation through the thickness. For the loading angles 10° compression, 0°, 10° tension the difference in stress triaxiality of material points

in the centre and on the outer surface of specimens is not significant. For these loading angles, the locations with high triaxiality values are used for the calibration. Under loading angle 20°, stress triaxiality and equivalent plastic strain compete each other (Fig. 8). For this loading angle the calibration is done according to the location with highest triaxiality value. Under 60° loading angle, through the thickness the difference of equivalent plastic strain is not significant. For that reason the material point in the middle is used for calibration.

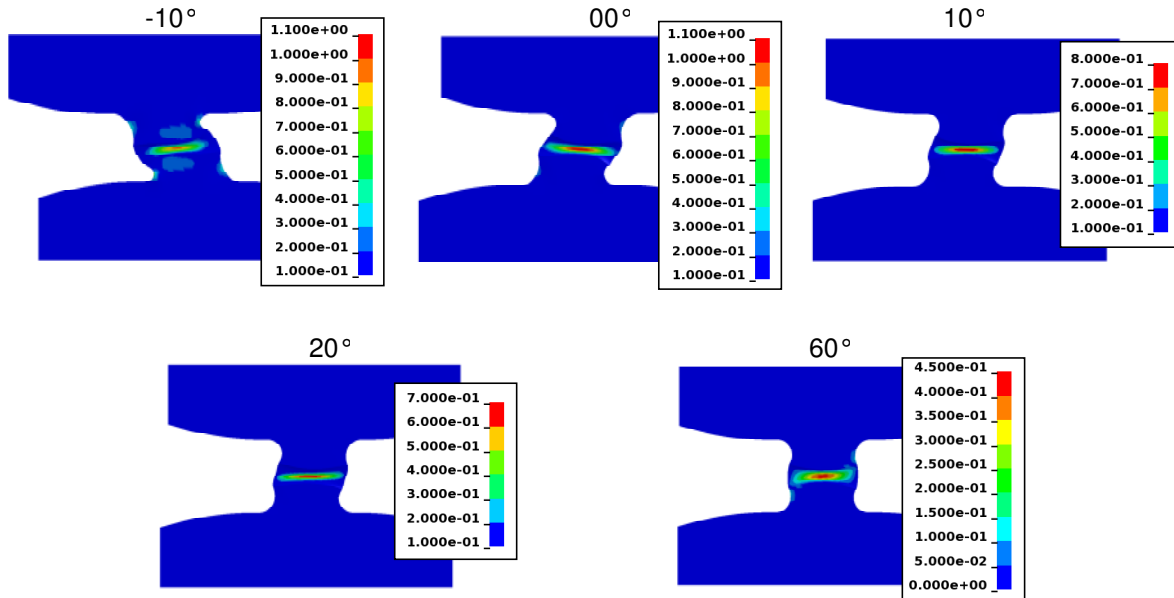


Figure 7: Equivalent plastic strain distribution just before the crack initiation on the butterfly specimens for different loading directions.

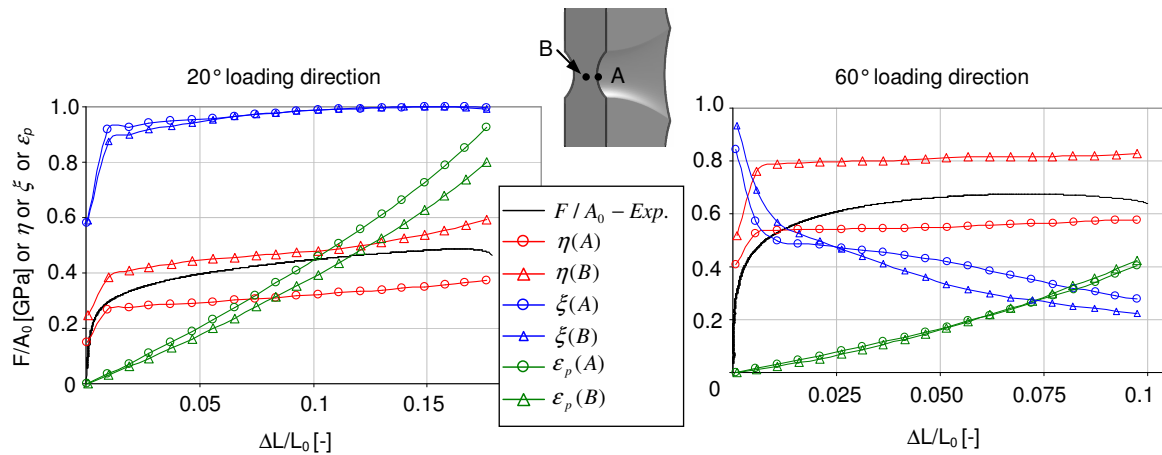


Figure 8: Evolution of stress triaxiality, Lode angle parameter and equivalent plastic strain to fracture at the centre of specimen and on the outer surface for the butterfly specimen with loading directions 20° and 60°

For many specimens the stress triaxiality and Lode angle parameter are not constant during plastic deformation. With the help of weighting functions discrete values for these two state parameters are calculated. The weight function f is defined by

$$f = \frac{n}{\varepsilon_f(\mu, \xi)} D^{\frac{1-n}{n}}, \quad (17.)$$

The weighted stress triaxiality and Lode angle parameter are described as

$$T_w = \frac{1}{D} \int_0^{\varepsilon_i} f T(\varepsilon_{pl}) d\varepsilon_{pl}, \quad (18.)$$

$$L_w = \frac{1}{D} \int_0^{\varepsilon_i} f L(\varepsilon_{pl}) d\varepsilon_{pl}, \quad (19.)$$

where ε_i is the maximum equivalent plastic strain for the integration. In case of integration to fracture strain, ε_i becomes ε_f and D becomes unity.

The damage does not necessarily accumulate linearly with equivalent plastic strain. In fact from micromechanical point of view the void formation and evolution are followed by a progressive void coalescence, which could be described as nonlinear damage accumulation. Some research showed experimentally that damage accumulates in nonlinear way. Bridgman carried out stepwise experiments for ductile steel under different hydrostatic pressures [28, page 79]. Using Bridgman's stepwise experiments for ductile steel, Xue [29] calculated the damage exponent $n = 2.21$ for a similar damage accumulation formulation with the assumption of constant stress triaxiality to fracture. Also Bonora [30] showed that the damage accumulation is not linear and damage rate is increasing with straining the material for 3 different types of ductile steel [30]. Weck and Wilkinson [31] used drilled metal sheets in order to investigate the void (damage) evolution and also found that damage evolution is not linear with respect to plastic strain. In this paper, as an assumption nonlinear damage accumulation with damage exponent $n = 2$ is used.

Evolution of stress triaxiality and Lode angle parameter with respect to equivalent strain at the crack initiation locations for butterfly specimens are shown in Fig. 9. The equivalent plastic strain at critical locations at crack initiation are plotted as squares for three experiments for each loading angles (-10°, 0°, 10°, 20° and 60°). For the calibration, from 3 tests one showing intermediate value has been used.

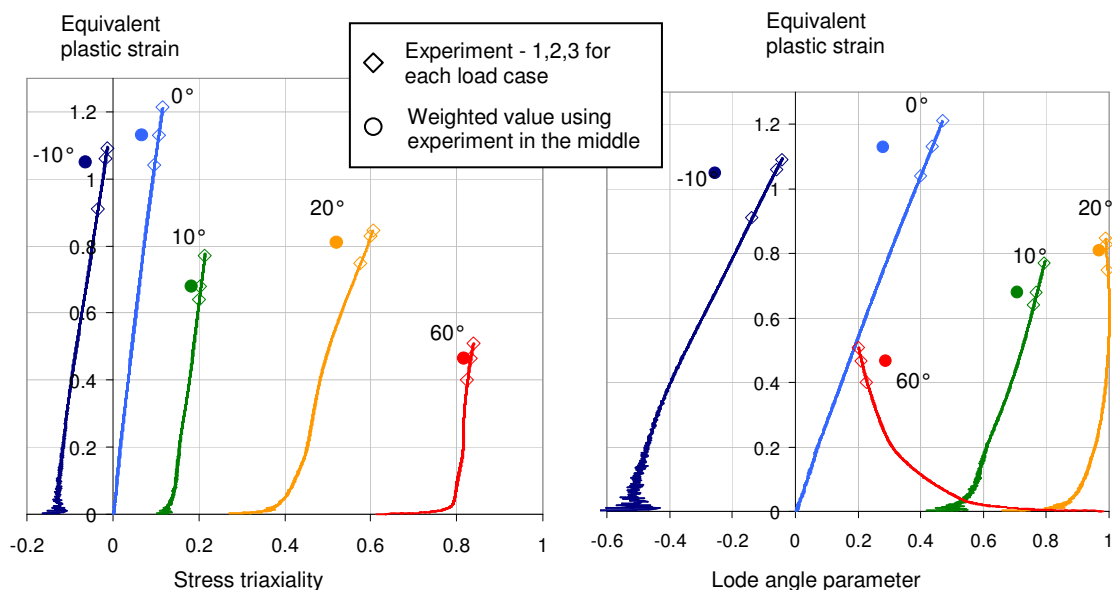


Figure 9: Evolution of the stress triaxiality, Lode angle parameter and equivalent plastic strain for butterfly specimens. For each load case three experiments are plotted with squares and the calculated weighted value according to middle experimental equivalent plastic strain at fracture

As stated, each specimen represents a point defined by the stress triaxiality, Lode angle parameter and fracture strain. For the current research there are no experimental results for the negative stress triaxiality. It has been showed by many researches that fracture strains for negative stress triaxiality values are very high. Bao [32] defined a cut-off negative triaxiality at stress triaxiality $-1/3$, below which material never fails. For the current research, there is no experimental data for negative stress triaxiality values and the material is assumed to fail at a fracture strain value 5 for stress triaxiality $-1/3$. An exponential trend in stress triaxiality direction is observed for the flat-grooved specimens and round

specimens. The fracture strain at high stress triaxiality range is assumed to follow the exponential trend obtained from the experiments mentioned before. The fracture surface is generated in Matlab by using the existing points and assumptions and is shown in Fig. 10 and Fig. 11. It should be noted that the generated fracture surface on the stress triaxiality and Lode angle parameter is dependent on damage exponent.

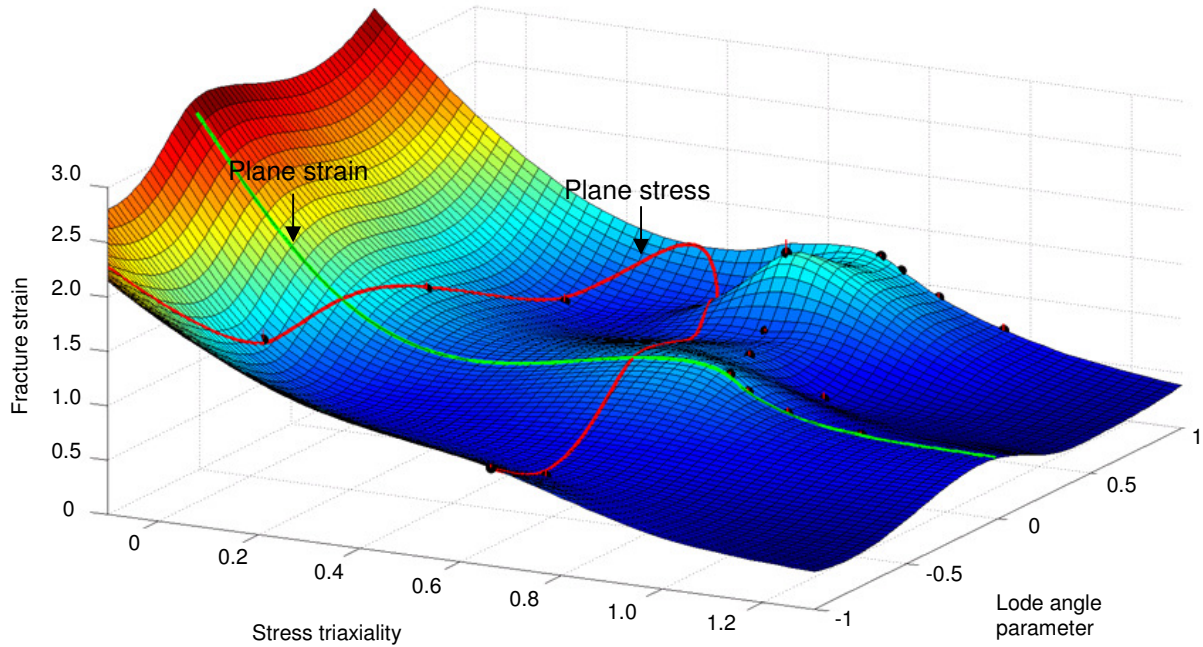


Figure 10: The generated fracture strain surface in stress triaxiality, Lode angle parameter and fracture strain space.

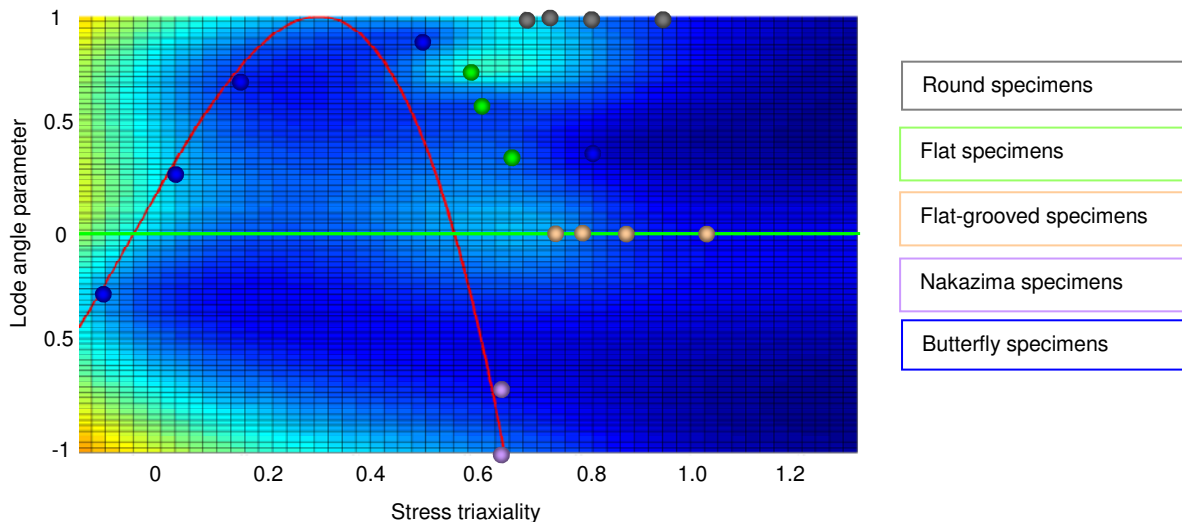


Figure 11: Illustration of fracture surface and stress states for different specimen groups.

6 Simulation of Specimens

Since some assumptions have been used, it is reasonable to simulate the experiments in order to check the accuracy of the calibration procedure. In the simulations, the extended GISSMO damage model (*MAT_ADD_EROSION) is coupled with von Mises plasticity (*MAT_024) and the created fracture surface is defined as table definition, which consists of stress triaxiality-fracture strain curves

for different Lode angle parameters. As mentioned above the damage is not coupled with plasticity. Comparison of experimental and numerical results for flat-grooved, round, butterfly, flat and Nakazima specimens are shown in Fig. 12-15. The numerical results agree with the experimental results well.

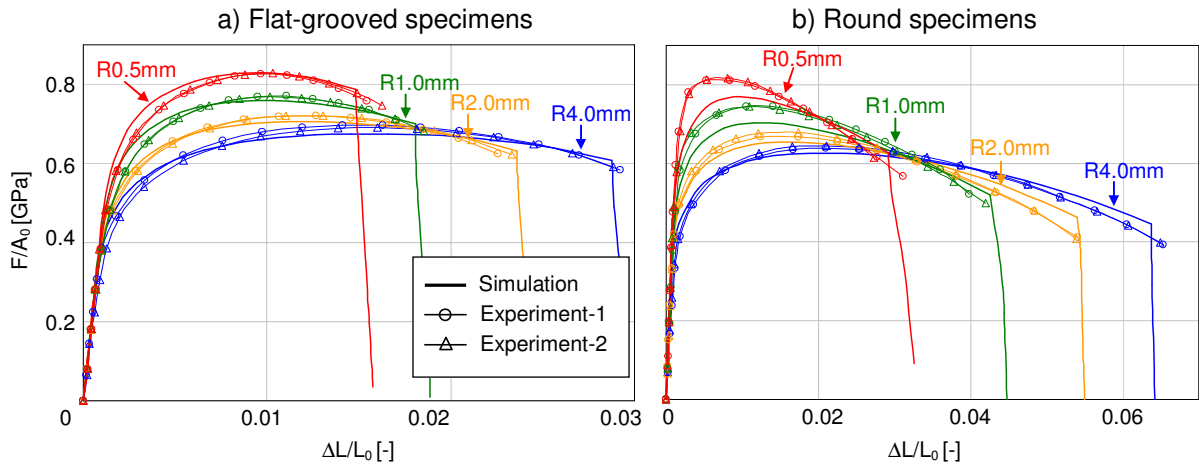


Figure 12: Comparison of force-displacement responses between numerical and experimental results for: a) flat-grooved specimens and b) round specimens with notches R0.5mm, 1mm, 2mm and 4mm.

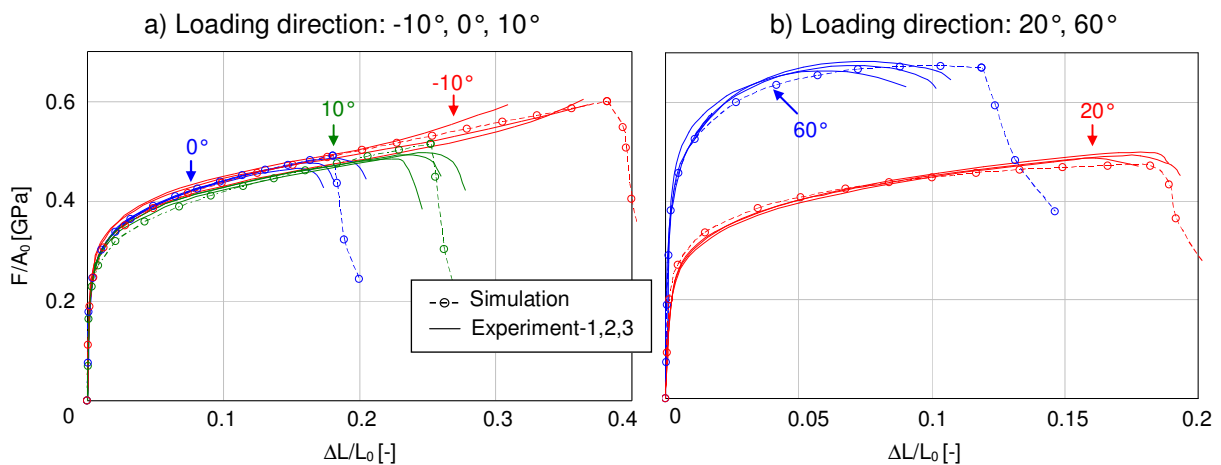


Figure 13: Comparison of numerical and experimental results for butterfly specimens with loading directions: a) -10° , 0° , 10° and b) 20° , 60° .

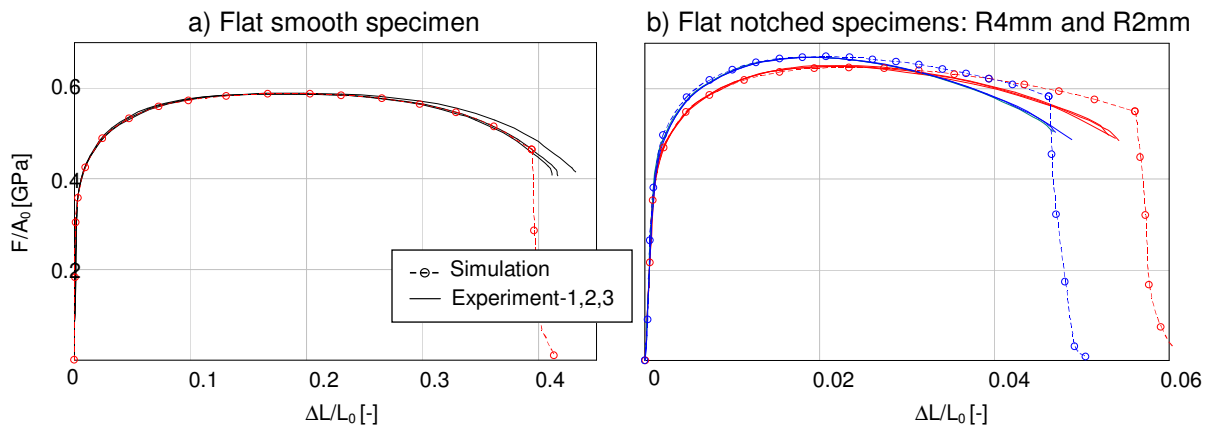


Figure 14: Comparison of numerical and experimental results for flat specimens: a) smooth and b) with notches R4mm and R2mm.

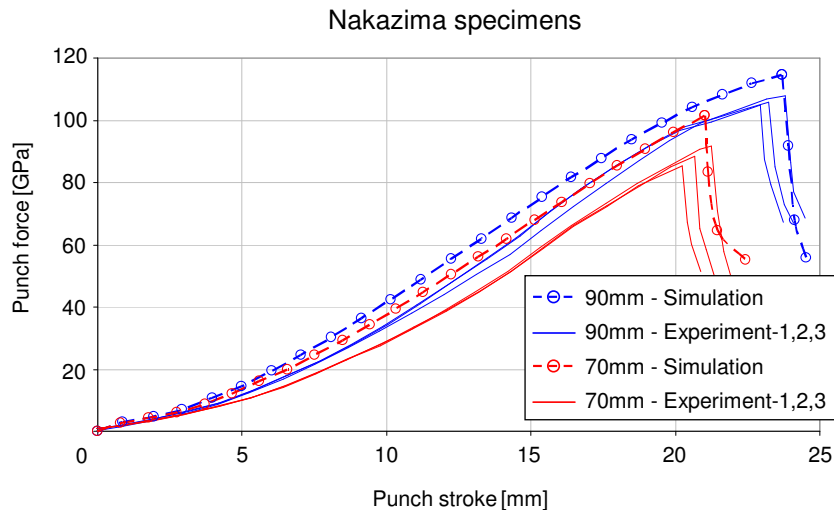


Figure 15: Comparison of force-displacement curves between numerical and experimental results for Nakazima tests.

7 Conclusion and Discussion

The Lode angle influence on fracture strain has been emphasized recently in the framework of continuum mechanics. The influence has been also shown experimentally for different materials using different specimen types. The focus of the present paper is on extension of the GISSMO damage model with consideration of Lode dependence and describing a calibration procedure depending on proper specimen types for dual phase steel DP600.

In order to define all stress states, in addition to stress triaxiality, the Lode angle dependence is also formulated with a dimensionless parameter. The stress triaxiality, Lode angle parameter space is covered with flat, round, flat-grooved plane strain, Nakazima and butterfly specimens. The proposed calibration method is carried out for the crack initiation locations. Weighting functions for the stress triaxiality and Lode angle parameter are defined since stress state parameters are not constant on the loading paths. The fracture strain surface is generated on the weighted values of stress state parameters of specimens. It has been observed that Lode angle parameter influence for DP600 is significant and should be considered in 3D simulations.

Current research is done using very fine discretization. Regularization issues with larger element lengths have to be researched further. In the present paper only quasi-static loading is considered. However, in crash simulations the components are subjected to different strain rates, and therefore, possible effects of strain rate on the fracture strain surface is another topic for future investigation.

In the present research, nonlinear damage accumulation with respect to equivalent plastic strain is considered. The generated fracture surface depends on damage exponent. Thus well designed multi step experiments with constant stress state parameters at crack initiation points or new experimental techniques to determine damage exponents are of great interest.

8 Acknowledgment

Thanks to Paul Du Bois for advice from his wealth of experience in crash simulation.

9 References

- [1] GR Johnson and WH Cook. Fracture Characteristics of Three Metals Subjected to Various Strains, Strain Rates, Temperatures and Pressures; *Engng. Fracture Mechanics*, 21(1):31, 1985.
 - [2] ML Wilkins, RD Streit, and JE Reaugh. Cumulative-strain-damage model of ductile fracture: simulation and prediction of engineering fracture tests. Technical report, Lawrence Livermore National Laboratory, Science Applications Inc, 1980.
 - [3] G. Rousselier. Ductile fracture models and their potential in local approach of fracture. *Nuclear engineering and design*, 105(1):97–111, 1987.
 - [4] AL Gurson. Continuum theory of ductile rupture by void nucleation and growth. Part I. Yield criteria and flow rules for porous ductile media. Technical report, COO-3084/39, Brown Univ., Providence, RI (USA). Div. of Engineering, 1975.
 - [5] J. Lemaitre. A continuous damage mechanics model for ductile fracture. *Journal of Engineering Materials and Technology*, 107:83, 1985.
 - [6] L. Xue. Stress based fracture envelope for damage plastic solids. *Engineering Fracture Mechanics*, 76(3):419–438, 2009.
 - [7] T. Wierzbicki and L. Xue. On the effect of the third invariant of the stress deviator on ductile fracture. Technical report, Impact and Crashworthiness Laboratory, Massachusetts Institute of Technology, Cambridge, MA, 2005.
 - [8] I. Barsoum and J. Faleskog. Rupture mechanisms in combined tension and shear-Micromechanics. *International Journal of Solids and Structures*, 44(17):5481–5498, 2007.
 - [9] L. Xue. Constitutive modeling of void shearing effect in ductile fracture of porous materials. *Engineering Fracture Mechanics*, 75(11):3343–3366, 2008.
 - [10] K. Nahshon and JW Hutchinson. Modification of the Gurson model for shear failure. *European Journal of Mechanics-A/Solids*, 27(1):1–17, 2008.
 - [11] Y. Bai and T. Wierzbicki. A new model of metal plasticity and fracture with pressure and Lode dependence. *International Journal of Plasticity*, 24(6):1071–1096, 2008.
 - [12] F. Neukamm, M. Feucht, and A. Haufe. Consistent damage modelling in the process chain of forming to crashworthiness simulations. *LS-DYNA Anwenderforum*, 2008.
 - [13] F. Neukamm, M. Feucht, and A. Haufe. Considering damage history in crashworthiness simulations. *LS-DYNA Anwenderforum*, 2009.
 - [14] F.A. McClintock, S.M. Kaplan, and C.A. Berg. Ductile fracture by hole growth in shear bands. *International Journal of Fracture*, 2(4):614–627, 1966.
 - [15] DM Rice et al. On the ductile enlargement of voids in triaxial stress fields** 1. *Journal of the Mechanics and Physics of Solids*, 17(3):201–217, 1969.
 - [16] Y. Bao and T. Wierzbicki. On fracture locus in the equivalent strain and stress triaxiality space. *International Journal of Mechanical Sciences*, 46(1):81–98, 2004.
 - [17] N.S. Ottosen and M. Ristinmaa. *The mechanics of constitutive modeling*. Elsevier Science Ltd, 2005.
 - [18] T. Wierzbicki and L. Xue. On the effect of the third invariant of the stress deviator on ductile fracture. Technical report, Impact and Crashworthiness Laboratory, Massachusetts Institute of Technology, Cambridge, MA, 2005.
 - [19] S. Murakami. Mechanical modeling of material damage. *Journal of Applied Mechanics*, 55:280, 1988.
 - [20] JL Chaboche. Anisotropic creep damage in the framework of continuum damage mechanics. *Nuclear Engineering and Design*, 79(3):309–319, 1984.
 - [21] M. Brünig. An anisotropic ductile damage model based on irreversible thermodynamics. *International Journal of Plasticity*, 19(10):1679–1713, 2003.
 - [22] S. Sommer and D. Sun. Charakterisierung und Modellierung der Tragfähigkeit von punktgeschweißten Stahlblechverbindungen unter Crashbelastung mit Hilfe von erweiterten Schädigungsmodellen. Technical report, Fraunhofer Institute for Mechanics of Materials IWM, 2006.
 - [23] JW Hancock and AC Mackenzie. On the mechanisms of ductile failure in high-strength steels subjected to multi-axial stress-states. *Journal of the Mechanics and Physics of Solids*, 24(2-3):147–60, 1976.
 - [24] D. Mohr and R. Treitler. Onset of fracture in high pressure die casting aluminum alloys. *Engineering Fracture Mechanics*, 75(1):97–116, 2008.
 - [25] W. Ramberg and W.R. Osgood. Description of stress-strain curves by three parameters. *Technical note*, 902, 1943.
 - [26] HW Swift. Plastic instability under plane stress. *Journal of the Mechanics and Physics of Solids*, (1):1–18, 1952.
-

- [27] P. Ludwik. *Elemente der technologischen Mechanik*. Springer, 1909.
- [28] P.W. Bridgman. *Studies in large plastic flow and fracture*. McGraw-Hill New York, 1952.
- [29] L. Xue. *Ductile fracture modelling: theory, experimental investigation and numerical verification*. PhD thesis, Massachusetts Institute of Technology, 2007.
- [30] N. Bonora. A nonlinear CDM model for ductile failure. *Engineering Fracture Mechanics*, 58(1-2):11–28, 1997.
- [31] A. Weck and DS Wilkinson. Experimental investigation of void coalescence in metallic sheets containing laser drilled holes. *Acta Materialia*, 56(8):1774–1784, 2008.
- [32] Y. Bao and T. Wierzbicki. On the cut-off value of negative triaxiality for fracture. *Engineering fracture mechanics*, 72(7):1049–1069, 2005.